Available online at www.sciencedirect.com
SCIENCE DIRECT®
Nuclear Instruments and Methods in Physics Research A 537 (2005) 537–561
NUCLEAR INSTRUMENTS & METHODS IN PHYSICS RESEARCH Section A
www.elsevier.com/locate/nima

Hadron and jet detection with a dual-readout calorimeter

N. Akchurin[a], K. Carrell[a], J. Hauptman[b], H. Kim[a], H.P. Paar[c], A. Penzo[d], R. Thomas[a], R. Wigmans[a,*]

[a]*Texas Tech University, Lubbock, TX 79409-1051, USA*
[b]*Iowa State University, Ames, USA*
[c]*University of California at San Diego, La Jolla, USA*
[d]*INFN Trieste, Italy*

Received 1 April 2004; received in revised form 7 July 2004; accepted 15 July 2004
Available online 11 September 2004

Abstract

Hadronic shower development in a copper-based fiber calorimeter is studied by simultaneously measuring the scintillation light and the Cherenkov light generated in this process. By comparing these two signals, the electromagnetic shower fraction can be measured event by event. Fluctuations in this fraction are the dominant contribution to the hadronic energy resolution. They are also responsible for the signal non-linearity and the non-Gaussian response function typical for hadron calorimeters. The dual-readout technique makes it possible to eliminate the effects of these fluctuations.

PACS: 29.40.Ka; 29.40.Mc; 29.40.Vj

Keywords: Sampling calorimetry; Hadron showers; Cherenkov light; Optical fibers

1. Introduction

In the past decades, detectors measuring the properties of particles by total absorption (calorimeters) have become crucial components of almost every experiment in high-energy particle physics. Whereas the detection of electrons, photons and other particles that develop electromagnetic showers can be performed with high precision, the same is not true for particles that are subject to the strong interaction. This is primarily due to the fact that

- the calorimeter typically generates a larger signal per unit deposited energy for the electromagnetic (em) shower component (primarily

*Corresponding author. Tel.: +1-806-742-3779; fax: +1-806-742-1182.
E-mail address: wigmans@ttu.edu (R. Wigmans).

0168-9002/$ - see front matter © 2004 Elsevier B.V. All rights reserved.
doi:10.1016/j.nima.2004.07.285

initiated by the process $\pi^0 \to \gamma\gamma$) than for the non-electromagnetic one (i.e. $e/h > 1$), and
- the fluctuations in the energy sharing between these two components are large and non-Poissonian.

As a result, in typical instruments the hadronic response function is non-Gaussian, the hadronic signals are non-linear, and the hadronic energy resolution exhibits substantial deviations from $E^{-1/2}$ scaling [1].

There are several ways to deal with the problems caused by this:

(1) *Compensating calorimeters* are designed to deliver equal response[1] to the em and non-em shower components: $e/h = 1$. Therefore, fluctuations in the energy fraction carried by the em shower component, f_{em}, are eliminated *by design*. This can be achieved in calorimeters with a hydrogenous active medium that is very sensitive to the soft neutrons abundantly produced in hadronic shower development. Such calorimeters require a precisely tuned sampling fraction. Since this sampling fraction is typically small (e.g., 2.3% in lead/plastic-scintillator calorimeters [2]), the em energy resolution of such devices is in practice limited to $\sim 15\%/\sqrt{E}$ [1].

(2) *Off-line compensation* is a technique applied in devices with $e/h \neq 1$, in which signals from different longitudinal sections of the calorimeter are weighted [3]. However, it has been shown that such methods may introduce a variety of undesirable side-effects [4].

(3) In the *Energy Flow method*, the calorimeter information is combined with measurements from a tracking system, to improve the performance for jets [5]. Using such methods, the ALEPH Collaboration improved their hadronic energy resolution (σ/E) from $85\%/\sqrt{E}$ for the calorimeter system alone to $60\%/\sqrt{E}$, for jets from Z_0 decay [6]. Similar improvements were obtained by the other LEP experiments. In a recent study, it was estimated that the relative improvement in the energy resolution achievable in a typical colliding-beam environment without the benefits of energy constraints is $\sim 30\%$ [7].

(4) *Measurement of the em shower component*, f_{em}, event by event through the spatial profile of the developing showers. Especially in detectors based on high-Z absorber material, these profiles are very different for em and hadronic showers and this method has been successfully applied for single particles [8]. However, the distinction becomes very problematic in high-energy jets, which consist of a *collection* of photons and hadrons entering the detector in an area with a size comparable to the lateral shower dimensions and/or the granularity of the detector.

In this paper, we report on yet another method. Since the resolution is determined by *fluctuations* in f_{em}, measurement of the f_{em} value *event by event* is the key to improving the hadronic energy resolution of an intrinsically non-compensating calorimeter. In our method, f_{em} is measured by comparing the shower signals produced in the form of scintillation light and Cherenkov light in one and the same detector. The idea for this approach originated from studies of calorimeters using quartz fibers as the active medium [9]. The signals in such detectors are generated by Cherenkov light. Hadrons showering in such detectors register, for all practical purposes, only through their em shower component, i.e. π^0 and η induced em showers completely dominate the hadronic signals. The non-em shower component is suppressed by a factor of about 5: $e/h \approx 5$ [9].

This result illustrates that the signals from the non-em component of hadron showers are strongly dominated by spallation protons produced in nuclear reactions. These particles are usually not sufficiently relativistic to produce Cherenkov light. The electrons and positrons through which the energy of the em shower component is deposited are relativistic down to a fraction of 1 MeV and thus dominate the production of Cherenkov light in hadron showers [1].

[1] Following the convention introduced in Ref. [1], we use the term *response* in this paper to indicate the average calorimeter signal per unit of deposited energy. The calorimeter response is normalized to 1 for em showers.

The calorimeter described in this paper exploits these phenomena. The detector is equipped with both scintillating fibers and fibers that only register Cherenkov light. Hadron showers developing in this detector generate signals in both types of fibers and these signals provide *complementary information* about these showers. The scintillating fibers produce light for every charged shower particle that crosses them. The amount of scintillation light is, in first approximation, proportional to dE/dx, the energy deposited by the shower particles in these fibers. On the other hand, the Cherenkov fibers only produce light when they are traversed by charged particles traveling faster than c/n, the local speed of light. Because of the dominant role of soft shower electrons, the amount of light in the Cherenkov fibers is a measure of the energy carried by π^0s and ηs produced in the shower development. By measuring the signals from both types of fibers simultaneously, one therefore learns (a) how much energy was deposited in the calorimeter and (b) what fraction of that energy was carried by the em shower component. With this method, the dominant source of fluctuations contributing to the hadronic energy resolution can thus be eliminated, since it allows a measurement of the em energy fraction, f_{em}, event by event.

The benefits of using this type of complementary information were first demonstrated in a prototype study for ACCESS, a high-energy cosmic ray experiment proposed for the International Space Station [10]. It was shown to be possible to estimate the effects of shower leakage, which dominate the performance of a very thin (25 cm of lead) calorimeter, by comparing the two signals. The fact that the dual-readout technique already worked so well in this very thin detector, which only looked at the initial part of the hadronic shower development, was an important inspiration for the 10 λ_{int} deep calorimeter we constructed for the present studies. The overwhelming majority of the non-relativistic shower particles, in particular the spallation and recoil protons, are produced in later stages of the hadronic shower development. The signals from these non-relativistic shower particles are crucial for the success of our method, since they are the ones that do produce scintillation light and no Cherenkov light.

This paper is organized as follows. In Sections 2 and 3, we describe the DREAM calorimeter and the experimental setup in which it was tested. In Section 4, the experimental data and the methods used to analyze these data are presented. The results are discussed in Section 5. Conclusions are summarized in Section 6.

2. The DREAM detector

The measurements described in this paper were performed with a calorimeter that has become known by its acronym DREAM, for Dual-REAdout Module. The basic element of this detector (see Fig. 1) was an extruded copper rod, 2 m long and $4 \times 4\,mm^2$ in cross-section. This rod was hollow, the central cylinder had a diameter of 2.5 mm. In this hole were inserted seven optical fibers. Three of these were plastic scintillating fibers,[2] the other four fibers were undoped. The latter were intended for detecting Cherenkov light and, therefore, we will refer to these in the following as *Cherenkov fibers*. We used two different types of Cherenkov fibers. For the central region of the detector, high-purity quartz fibers[3] were used, while the peripheral regions of the detector were equipped with acrylic plastic fibers.[4] The latter were a factor of 20 cheaper. All fibers had an outer diameter of 0.8 mm and a length of 2.50 m. The fiber pattern was the same for all rods, and is shown in Fig. 1.

The DREAM detector consisted of 5580 such rods, 5130 of these were equipped with fibers. The empty rods were used as fillers, on the periphery of the detector. The instrumented volume thus had a length of 2.0 m, an effective radius of $\sqrt{5130 \times 0.16/\pi} = 16.2$ cm, and a mass of 1030 kg. The effective radiation length (X_0) of the calorimeter was 20.1 mm, the Molière radius (ρ_M) was 20.4 mm and the nuclear interaction length (λ_{int}) 200 mm. The composition of the instrumented part of the calorimeter was as follows: 69.3% of the detector volume consisted

[2]SCSF-81J, produced by Kuraray Co. Ltd, Tokyo, Japan.

[3]Polymer-clad fused silica fibers, produced by Polymicro, Phoenix, Arizona, USA.

[4]Raytela PJR-FB750, produced by Toray, Japan.

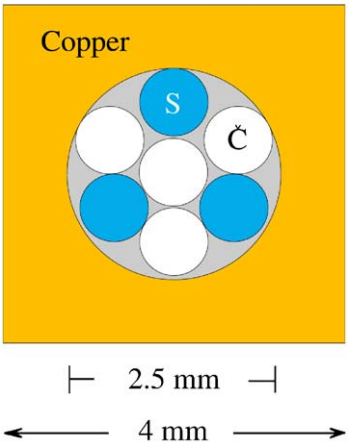

Fig. 1. The basic building block of the DREAM detector is a $4 \times 4\,mm^2$ extruded hollow copper rod of 2 meters length, with a 2.5 mm diameter central hole. Seven optical fibers (four Cherenkov and three scintillating fibers) with a diameter of 0.8 mm each are inserted in this hole.

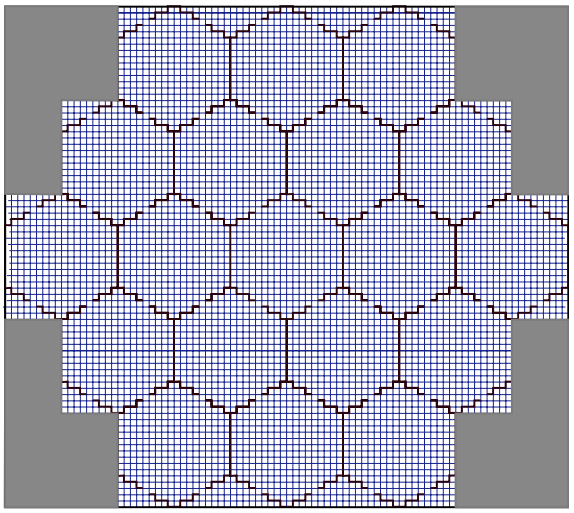

Fig. 2. Layout of the DREAM detector.

of copper absorber, while the scintillating and Cherenkov fibers occupied 9.4% and 12.6%, respectively. Air accounted for the remaining 8.7%. Given the specific energy loss of a minimum-ionizing particle (mip) in copper (12.6 MeV/cm) and polystyrene (2.00 MeV/cm), the sampling fraction of the copper/scintillating-fiber structure for mips was thus 2.1%.

The fibers were grouped to form 19 towers. Each tower consisted of 270 rods and had an approximately hexagonal shape (80 mm apex to apex). The layout is schematically shown in Fig. 2: a central tower, surrounded by two hexagonal rings, the Inner Ring (6 towers) and the Outer Ring (12 towers). The towers were longitudinally unsegmented.

The depth of the copper structure was 200 cm, or $10.0\lambda_{int}$. The fibers leaving the rear of this structure were separated into bunches: One bunch of scintillating fibers and one bunch of Cherenkov fibers for each tower, 38 bunches in total. In this way, the readout structure was established (see Fig. 3). Each bunch was coupled through a 2 mm air gap to a photomultiplier tube (PMT).

We selected a 10-stage, 1.5 in PMT (Hamamatsu R-580) with a nominal gain of 3.7×10^5 at 1250 V. The larger gain needed for the readout of the Cherenkov fibers was obtained at approximately 1500 V, while the smaller gain needed for the readout of the scintillating fibers could not be reached by lowering the high voltage alone. Although the base with tapered voltage divider chosen (Hamamatsu E2183-501) was optimized for linearity, we did not want to lower the voltage so much that the linearity would be at risk. Thus we chose a high voltage of ~ 1000 V for the PMTs reading out the scintillating fibers and installed a yellow filter[5] between the fiber ends and the photocathode. To avoid a coupling capacitor in the anode signal path, we chose to have the anode near ground potential and the photocathode at negative high voltage. For best gain stability, we selected a PMT with an internal electrostatic shield surrounding the photocathode. This shield was held at the same potential as the photocathode. The PMT was surrounded by a high-permeability (10^5) μ-metal shield surrounded by a 5 mm thick iron shield. The μ-metal shield protruded more than 3.5 cm and the iron shield 5 cm in forward of the photocathode. This provided stability of the PMT gain when the beam tests required the

[5]Kodak, Wratten #3, nominal transmission 7% at 425 nm, 90% at 550 nm.

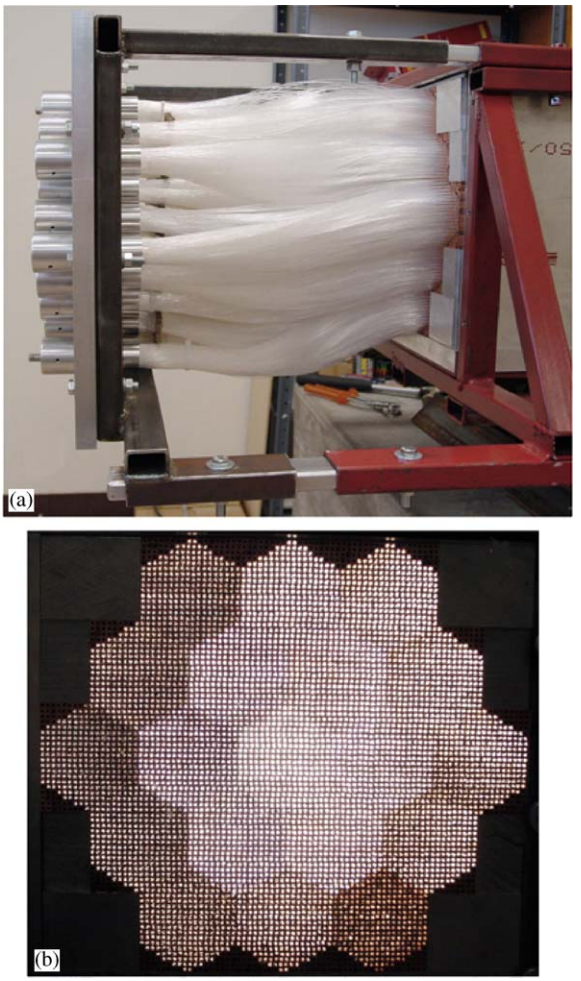

Fig. 3. The DREAM detector. Shown are the fiber bunches exiting from the rear face of the detector (a) and a picture taken from the front face while the rear end was illuminated (b).

calorimeter to be rotated and thus the direction of the Earth's magnetic field changed.

The yellow filter further had the advantage that it increased the attenuation length of the scintillating fibers substantially [11]. The blue part of the spectrum of light generated in the scintillating fibers is attenuated by self-absorption (resulting from overlap between the emission and absorption bands) and the yellow filter predominantly removed that part of the spectrum. The Cherenkov fibers did not suffer from significant longitudinal non-uniformity, their light attenuation characteristics were adequate without filtering (see Section 4.3).

Fig. 3 shows photographs of the assembled detector. In Fig. 3a, the fiber bunches exiting the downstream end of the calorimeter and the 38 PMTs used to detect their signals are shown. In total, this detector contained about 90 km of optical fibers. Fig. 3b shows the front face of the calorimeter, when the fibers were illuminated with a bright lamp in the rear. The hexagonal readout structure is clearly visible.

3. Experimental setup

3.1. The beam line

The measurements described in this paper were performed in the H4 beam line of the Super Proton Synchrotron at CERN. The DREAM detector was mounted on a platform that could move vertically and sideways with respect to the beam. Changing the angle of incidence of the beam particles with respect to the fibers in the horizontal plane (the ϕ angle) and the vertical plane (the tilt angle, θ) was achieved with a crane. For the hadron and jet measurements described in this paper, we used two detector orientations. In position *A*, for which most data were collected, ϕ and θ were 2° and 0.7°, respectively. In position *B*, also referred to as the *tilted* position, ϕ and θ were 3° and 2°, respectively.

The beam particle rates were typically several thousand per spill. The spills lasted 2.6 s and were repeated every 14.4 s. The widths of the collimators in the beam line were chosen so as to make the contribution of the momentum spread of the beam particles negligible. The purity of the electron beam varied considerably, depending on the energy and the chosen collimator settings. In particular, high-energy electron beams were contaminated with pions and muons.

We used several auxiliary detectors in the beam tests. These detectors served to obtain pure samples of incident particles and to measure the impact point of these particles in the calorimeter event by event. Fig. 4 shows a schematic view of the positioning of these detectors, which are described below.

Fig. 4. Schematic view of the experimental setup in the beam line in which the DREAM detector was tested.

3.1.1. The trigger counters

Two small scintillation counters provided the signals that were used to trigger the data acquisition system. These Trigger Counters (TC) were 2.5 mm thick, and the area of overlap was $6 \times 6\,\mathrm{cm}^2$. A coincidence between the logic signals from these counters provided the trigger.

3.1.2. The hodoscope

The impact point of the beam particles in the DREAM detector was measured with a fiber hodoscope (HOD). This hodoscope consisted of ribbons of scintillating fibers oriented in the horizontal or vertical direction, thus providing the y and x coordinates of the beam particles. The fibers were 500 μm thick. Their signals were read out by means of multi-anode PMTs.[6] This detector was installed about 3 m upstream of the front face of the DREAM calorimeter. Using the hodoscope information, it was possible to determine the coordinates of the impact point in the calorimeter with a precision of a fraction of 1 mm, depending on the beam energy. More details about this instrument, as well as examples of its excellent performance in these beam tests, are described elsewhere [12].

3.1.3. The preshower detector

The preshower detector (PSD) consisted of a 5 mm thick ($1X_0$) lead absorber, followed by a scintillation counter. This simple device turned out to be extremely useful to eliminate beam contamination and made it possible to obtain data samples of high purity. Fig. 5 shows the signal distribution for a 100 GeV electron beam. This beam contained some contamination from pions and muons, which were responsible for the minimum-ionizing peak in the PSD spectrum. Electrons started em showers in the $1X_0$ lead absorber and produced signals that were typically 10 times larger than those from mips. By requiring PSD signals smaller than 2 mips, electrons contaminating pion beams were effectively eliminated. More details about the performance of this instrument are given elsewhere [12].

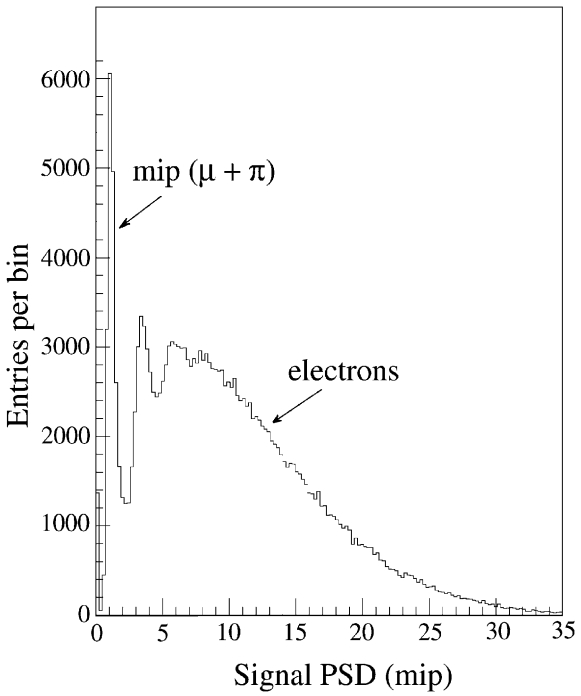

Fig. 5. Signal distribution for events recorded in the preshower detector for a 100 GeV electron beam.

3.1.4. The interaction target

For the measurements of single pions, the PSD was installed right in front of the DREAM

[6] Hamamatsu R2486, equipped with 16×16 anode wires for position detection.

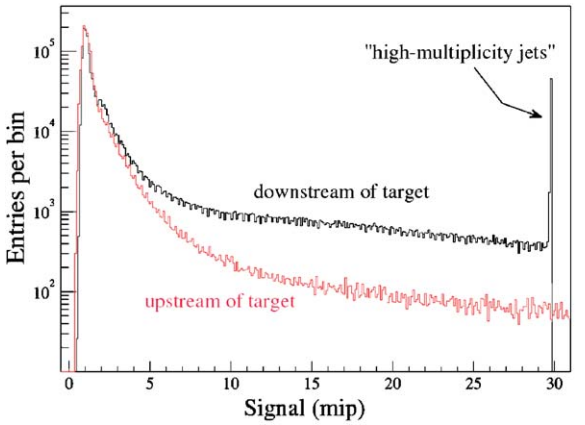

Fig. 6. Signal distributions for events recorded in the 200 GeV pion beam, in the scintillator planes upstream and downstream of the polyethylene interaction target (see Fig. 4).

calorimeter, at about 1 cm from its front face. However, for the studies of jets, the configuration was changed, as indicated in Fig. 4. A 10 cm thick polyethylene target ($\sim 0.1\lambda_{\rm int}$) was installed in front of the calorimeter. The PSD was moved upstream of this target, while an additional scintillation counter (ITC) was installed between the target and the calorimeter. With this setup, nuclear interactions of beam pions in the target could be selected, by requiring a mip signal in the upstream preshower detector (indicating the passage of a single pion) and a much larger signal in the downstream counter (ITC).

This is illustrated in Fig. 6, which shows signal distributions in the scintillator planes upstream and downstream of the polyethylene interaction target (see Fig. 4). The size of the latter signal is indicative for the multiplicity of the secondaries produced in this nuclear reaction.

The events created in this way are not representative of typical jets (i.e. , fragmenting quarks or gluons) studied in modern high-energy colliding-beam experiments. However, for purposes of calorimetry they are nevertheless useful. The reaction products constitute a collection of photons (from π^0 decay) and hadrons (mainly pions). Both the number and the nature of these particles fluctuate. This is the essential characteristic of jets that makes their detection different from that of mono-energetic hadrons. So even though the composition of the reaction products created this way is different from that of jets, this essential element is preserved. And, crucial from a measurement point of view, the *total energy* of the "jet" mimicked this way is known, so that the "jet" resolution can be experimentally determined. In the absence of a "jet test beam", this is the best way to measure the calorimeter performance for jet detection. However, one should keep in mind that, inevitably, some of the particles produced in the interactions are (partially) absorbed in the target. The fact that the calorimeter response to "jets" is systematically smaller than that to single pions of the same energy is indicative for such energy losses.

3.1.5. The muon detector

Downstream of the calorimeter, behind an additional $8\lambda_{\rm int}$ of absorber, a $30 \times 30\,{\rm cm}^2$ scintillation counter (MU) served to identify muons that contaminated the beam.

3.2. Data acquisition

The various detector signals were transported through RG-58 cables with (for timing purposes) appropriate lengths to the counting room. There, the signals to be digitized (i.e. all except those from the trigger counters and the fiber hodoscope) were fed into charge ADCs. Two types of ADCs were used for these tests. Both types had a sensitivity of 4 counts/pC. The signals from the central tower and the Inner Ring were digitized by 11-bit Lecroy 2249W ADCs, which have a range of 500 pC. The signals from the 12 towers constituting the Outer Ring were digitized by 10-bit Lecroy 2249 ADCs, which have a range of 250 pC. The duration of the gate opened by the trigger signal was 120 ns, and the calorimeter signals arrived ~ 30 ns after the start of the gate.

The signals from the fiber hodoscope were fed into TDCs. In total, eight TDCs were used, four for the horizontal and vertical fiber ribbons, respectively. The time information could be converted into (x, y) coordinates of the point where the beam particle traversed the hodoscope.

The data acquisition system was based on CAMAC, interfaced via a VME bus to a

Linux-based computer. At maximum, 8000 events could be recorded per 2.6 s SPS spill. The typical event size was ~ 150 bytes. All calorimeter signals, as well as the signals from all auxiliary detectors, could be monitored on-line.

3.3. Calibration of the detectors

Using the high voltage, the gain in the PMTs was set to generate $\sim 2\,\mathrm{pC/GeV}$ in the central detector tower, $\sim 4\,\mathrm{pC/GeV}$ in the Inner Ring and $\sim 6\,\mathrm{pC/GeV}$ in the Outer Ring of the DREAM calorimeter. By choosing different gains, we effectively extended the limited dynamic range of our readout and thus increased its sensitivity to small energy deposits in the shower tails.

Each of the 19 towers was calibrated with 40 GeV electrons. The average signal for 40 GeV electrons entering in the center of a tower corresponded to about 300, 600 or 900 ADC counts above the pedestal value in that tower, depending on the chosen gain. On average, 92.5% of the scintillator light and 93.6% of the Cherenkov light was generated in that tower [12]. The signals observed in the exposed tower thus corresponded to an energy deposit of 37.0 GeV in the case of the scintillating fibers and of 37.4 GeV for the Cherenkov fibers. This, together with the precisely measured values of the average signals from the exposed tower, formed the basis for determining the calibration constants, i.e. the relationship between the measured number of ADC counts and the corresponding energy deposit. The stability of the calibration was checked four times during the test period by sending 40 GeV electrons into the center of each calorimeter tower and measuring the signal distribution. The mean values of these distributions were reproduced to better than 2% in these measurements, for all channels and for the entire test period of seven days.

4. Experimental data and analysis methods

4.1. Experimental data

Events were triggered by coincident signals in the scintillation counters upstream of the calorimeter. Only events for which the (x, y) coordinates of the beam particle in the fiber hodoscope were measured were retained for the analyses described in this paper. One of the purposes of the hodoscope information was to limit the impact region of the beam particles. For the analyses described in this paper, a circular region with a radius of 1.0 cm was selected.

The following data sets were used for the analyses described in this paper:

(1) Negative pion data at 20, 40, 80, 100, 150, 200, 250 and 300 GeV, taken in the center of the DREAM calorimeter, with the detector oriented in the untilted position, $A(2^\circ, 0.7^\circ)$.
(2) Negative pion data at 50, 100, 200 and 300 GeV, taken in the center of the calorimeter, with the detector oriented in the tilted position, $B(3^\circ, 2^\circ)$.
(3) "Jet" data (see Section 3.1.4). High statistics runs (1 million triggers or more) in which π^- of 50, 100, 200 and 300 GeV were sent onto the interaction target. The beam was aimed at the center of the DREAM calorimeter, which was oriented in position $A(2^\circ, 0.7^\circ)$.

4.2. Event selection

A large fraction (90% or more) of the beam particles were of the desired type. The only contamination came from muons, which were effectively removed from the data samples by using the signals recorded in the muon counter downstream of the calorimeter and the additional $8\lambda_{\mathrm{int}}$ absorber. By requiring a signal compatible with a mip in the PSD scintillator plane, we also removed any eventual electron contamination, as well as pions that interacted upstream of that counter, e.g., in the 5 mm lead absorber of the PSD.

A small fraction of the pions penetrated at least one meter into the DREAM calorimeter before inducing a nuclear interaction that started the shower. These events could be recognized by exploiting the fact that the calorimeter was oriented at a small angle with the beam direction. By comparing the x-coordinate of the impact point of the particle, as derived from the hodoscope

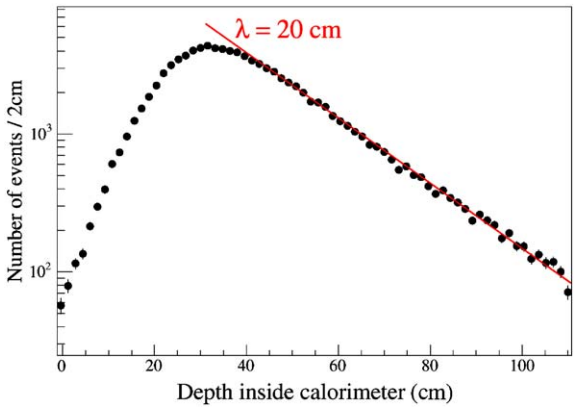

Fig. 7. Distribution of the depth of the center-of-gravity of the scintillation light produced in the DREAM calorimeter by 200 GeV π^-.

information, with the x-coordinate of the center-of-gravity of the energy deposit profile in the calorimeter, the depth of the latter center-of-gravity could be determined event by event.

Fig. 7 shows the number of 200 GeV π^- events as a function of the effective depth at which they generated scintillation light. The solid line drawn in this figure represents an exponential decrease with a slope of 20 cm, the nuclear interaction length of this detector: $f(z) \propto \exp(-z/20)$. The starting points of the hadron showers are distributed according to $f(z)$, and the experimental data plotted in this figure represent a convolution of the average longitudinal shower profile and $f(z)$.

In order to limit the effects of shower leakage on our results, we removed late-showering particles from the event samples. Only events in which the center-of-gravity of the light production was located in the first meter ($5\lambda_{\text{int}}$) were used in the analyses. This cut removed typically less than 5% of the events.

4.3. Corrections for light attenuation

Knowledge of the depth of the light production inside the DREAM calorimeter made it possible to correct the experimental data for the effects of light attenuation in the fibers. The light attenuation characteristics were measured in great detail by rotating the detector at an angle of 24° in the horizontal plane and measuring the signals from 40 GeV electron showers as a function of impact point along the full length of the fibers. These measurements are described in detail in Ref. [12]. The attenuation lengths of the 3 types of fibers used in the detector (scintillating, quartz and clear plastic) were found to be 5, 15 and 8 m, respectively. Since the Cherenkov light was predominantly produced in the quartz fibers, the effects of light attenuation on the Cherenkov signals was negligibly small. However, the effects of light attenuation in the scintillating fibers were noticeable.

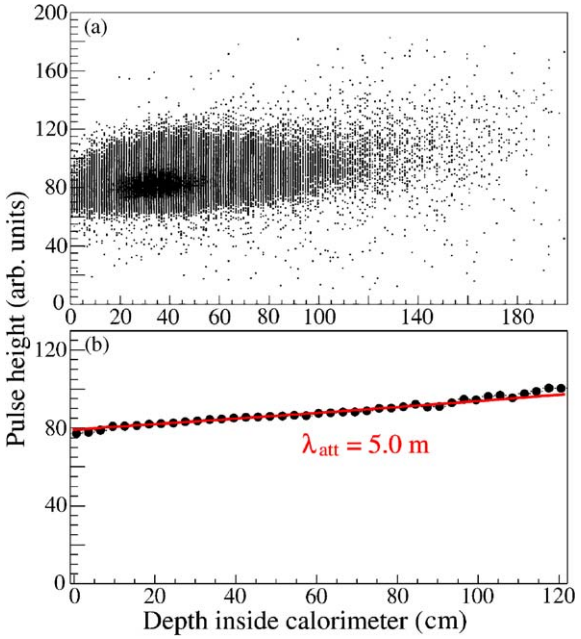

Fig. 8. Scatter plot showing the total scintillator signal vs. the average depth of the light production (a), and the average total scintillator signal as a function of that depth (b), for events induced by 100 GeV π^-. The curve is an exponential with a slope of 5 m (the measured attenuation length of the scintillating fibers), fitted to the data.

This is illustrated in Fig. 8. In Fig. 8a, the total calorimeter signal from the scintillating fibers is plotted vs. the average depth at which the scintillation light is generated, for each event. For most events, this point is located at a depth of ~ 40 cm, i.e. $2\lambda_{\text{int}}$. The data show that the signal gradually increases with depth. In Fig. 8b, the

average signal is shown as a function of the average depth at which it was generated. These data are well described with an exponential curve with a slope of 5 m, the measured attenuation length of the scintillating fibers.

In the analyses described in the next sections, the scintillator signals were corrected for the effects of light attenuation. All scintillator signals were multiplied by a factor $\exp[-(z_{\text{eff}} - 30)/500]$, where z_{eff} represents the average depth at which the scintillation light was generated for the event in question. In this way, the hadron signals were normalized to the ones produced by 40 GeV electrons, which were found to generate light at an average depth of 30 cm ($15X_0$). As discussed in Section 3.3, the signals from 40 GeV electrons were used to calibrate the detector. By following this procedure, hadron signals are thus expressed in the same units as the electron signals. The effects of this correction were small. On average, the scintillator signals were reduced by $\sim 2\%$. No corrections were applied for the Cherenkov signals.

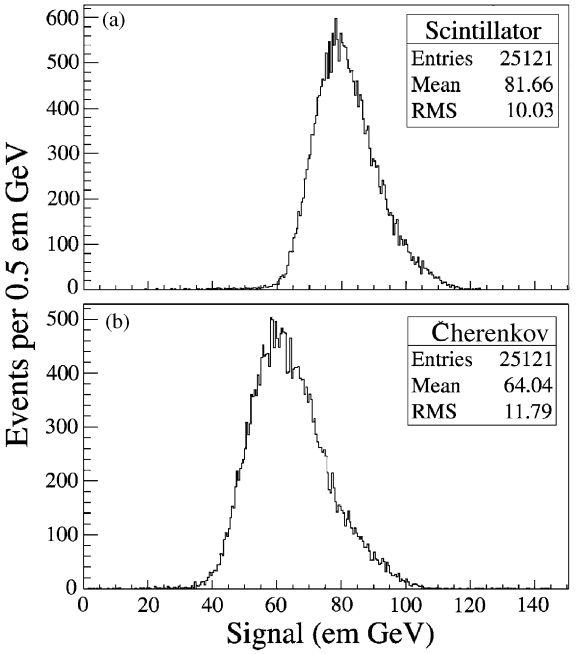

Fig. 9. Signal distributions for 100 GeV π^- recorded by the scintillating (a) and Cherenkov (b) fibers of the DREAM calorimeter, oriented in the untilted position, $A(2^\circ, 0.7^\circ)$. The signals are expressed in the same units as those for em showers, which were used to calibrate the detector (em GeV).

5. Experimental results

5.1. Single pions

We describe here some results obtained with negative pions with energies ranging from 20 to 300 GeV (data sets 1 and 2, described in Section 4.1).

Fig. 9 shows the signal distributions for 100 GeV π^- as measured with the scintillating (Fig. 9a) and Cherenkov (Fig. 9b) fibers, with the calorimeter oriented in the untilted position, $A(2^\circ, 0.7^\circ)$. These distributions exhibit the characteristics typical of non-compensating calorimeters:

- They are asymmetric,
- They are broad (with resolutions σ_{rms}/mean of 12.3% and 19.0%, respectively),
- The mean values are considerably smaller than those for electrons of the same energy, which were used to set the scale: 81.7 and 64.0 GeV for the scintillator and Cherenkov signals, respectively, vs. 100 GeV for electrons.

The energy dependence of the energy resolution is shown in Fig. 10. This resolution is well described by a *linear* sum of a $E^{-1/2}$ scaling term and a constant term (e.g., $\chi^2/N_{\text{dof}} = 7.0/6$ for the Cherenkov channel). The results of least-squares fits to the experimental points are indicated in the figure. We checked that a quadratic sum of two such terms does not describe the data well ($\chi^2/N_{\text{dof}} = 247/6$ for the Cherenkov channel), as expected for a calorimeter whose resolution is dominated by the effects of non-compensation [1].

The calorimeter is also considerably non-linear for pion detection. This is illustrated in Fig. 11, which shows the calorimeter response, in terms of scintillation light, as a function of the pion energy. Over the energy range covered by these experiments, the scintillator response increased by $\sim 20\%$.

The hadronic calorimeter response, either for the scintillation or the Cherenkov light, can be expressed in terms of the em shower fraction (f_{em})

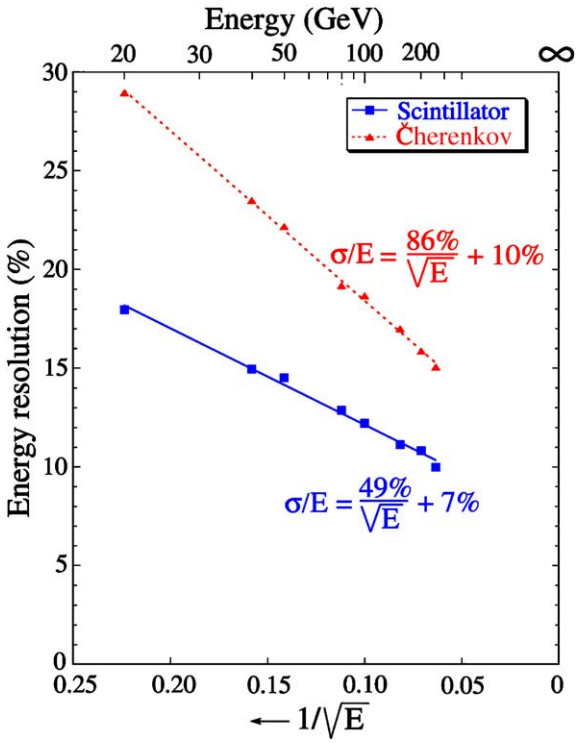

Fig. 10. The energy resolution of the DREAM detector for the scintillator and Cherenkov signals from single-pion showers, as a function of the pion energy. The lines represent the results of least-squares fits to the experimental data.

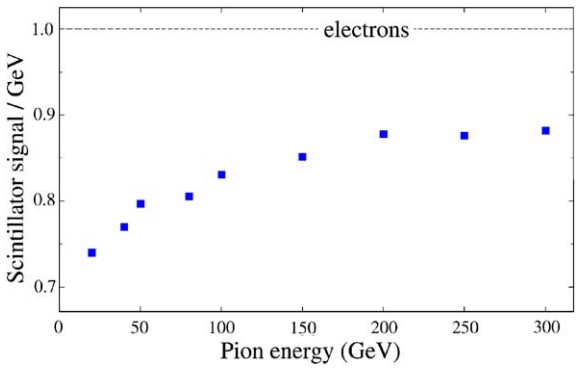

Fig. 11. The scintillator response of the DREAM calorimeter to pions, as a function of energy.

and the e/h ratio

$$R(f_{\mathrm{em}}) = f_{\mathrm{em}} + \frac{1}{e/h}(1 - f_{\mathrm{em}}). \quad (1)$$

Defined in this way, $R = 1$ for em showers. The e/h ratio, i.e. the ratio of the detector response to em and non-em shower components, depends on the choice of the passive and active calorimeter media and on the sampling fraction, i.e. on the ratio between the amounts of active and passive material.

This relationship holds separately for both sampling media. The differences between the scintillator and Cherenkov characteristics of the calorimeter derive from the fact that the e/h values are very different for these two media. The e/h value of a copper/quartz-fiber calorimeter was measured to be ~ 5 [9], while the e/h value of the copper/plastic-scintillator structure, which has a sampling fraction of 2.1%, is estimated to be 1.4, on the basis of the experience gained with iron/plastic-scintillator calorimeters [4].

The hadronic signal non-linearity is caused by the fact that the average value of f_{em} increases with incident energy, while the non-Poissonian event-to-event fluctuations in f_{em} are reflected in the characteristic asymmetric line shapes (Fig. 9). The much larger e/h ratio for the Cherenkov structure is responsible for its smaller response and its worse energy resolution. The data from Fig. 10 clearly show that the e/h value affects not only the energy independent term, but also the coefficient of the $E^{-1/2}$ scaling term in the energy resolution [1].

As we argued in Section 1, knowledge of the value of f_{em} on an event-by-event basis is the key to eliminating these undesirable effects and thus improving the calorimeter performance. Because of the large difference between the e/h values for the copper/plastic-scintillator and copper/Cherenkov structures, simultaneous measurements of the two signals provides this information.

Fig. 12 shows a scatter plot of the Cherenkov signals (Q) versus the scintillator signals (S), for the 100 GeV π^- sample. The distributions of the scintillator and Cherenkov signals shown in Fig. 9 are the projections of this scatter plot on the horizontal and vertical axes, respectively. There are several ways in which one can combine the information from the two signals to reduce

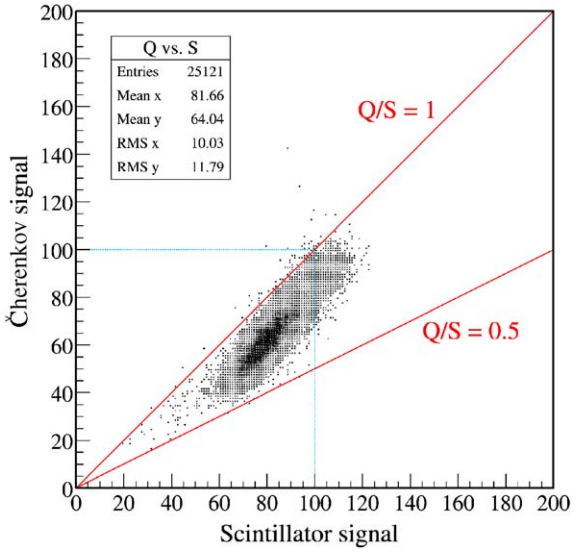

Fig. 12. Cherenkov signals versus scintillator signals for 100 GeV π^-.

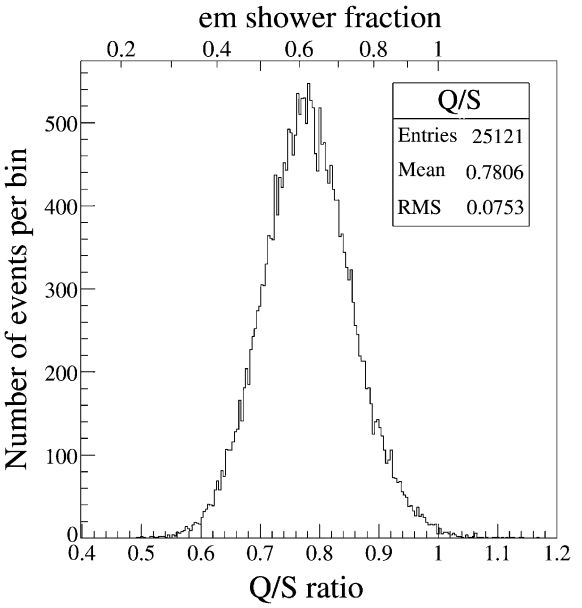

Fig. 13. Distribution of the Q/S signal ratio, and the em shower fraction derived on the basis of Eq. (2), for 100 GeV π^- detected with the DREAM calorimeter.

the width(s) of these projected spectra, i.e. the energy resolution.

One variable that is directly related to f_{em} is the Q/S signal ratio. Based on Eq. (1), this ratio can be written as

$$\frac{Q}{S}=\frac{f_{em}+0.20\ (1-f_{em})}{f_{em}+0.71\ (1-f_{em})} \tag{2}$$

since $(e/h)^{-1}=0.20$ and 0.71 for the Cherenkov and scintillator readout, respectively. Two lines drawn in Fig. 12 are representing $Q/S=1$ and 0.5. Fig. 13 shows the measured distribution of the Q/S signal ratio. The average value of this ratio is 0.78 at 100 GeV. The fact that the Q/S ratio is smaller than 1.0 thus indicates that a significant fraction, typically $\sim 25\%$, of the scintillator signal from the pions showering in this detector is caused by *non-relativistic* particles, predominantly protons released from nuclei in spallation processes, or recoiling from elastic neutron scattering in the plastic fibers.

The top axis of Fig. 13 shows the em shower fraction, f_{em}, which is related to the Q/S signal ratio through the expression given in Eq. (2), assuming e/h values of 1.4 and 5 for the two active media. Under these assumptions, about 60% of the shower energy is, on average, carried by the em shower component at this energy.

We return to the use of the Q/S ratio in Section 5.3. Here, we use another variable to improve the calorimeter performance: $(Q+S)/E$, where E represents the nominal beam energy. As can be seen from Eq. (1), this variable is also related to f_{em}, as

$$\frac{(Q+S)}{E}=0.91+1.09f_{em} \tag{3}$$

using $e/h=5$ and 1.4 for the Q and S signals, respectively. The distribution of this variable, for events induced by 100 GeV π^-, is shown in Fig. 14a. The top axis gives the scale for f_{em}. Unlike Q/S, the variable $(Q+S)/E$ has a linear relationship with f_{em}. Therefore, the distribution in Fig. 14a exhibits the non-Poissonian, asymmetric fluctuations characteristic of the em shower fraction.

In Fig. 14b, the average scintillator signal for 100 GeV π^- showers is shown as a function of $(Q+S)/E$, i.e. f_{em}. In the region $0.9<(Q+S)/E<2.0$, i.e. $0<f_{em}<1$, the relationship is described by means of a straight line. We have used the results of this fit to apply a correction to

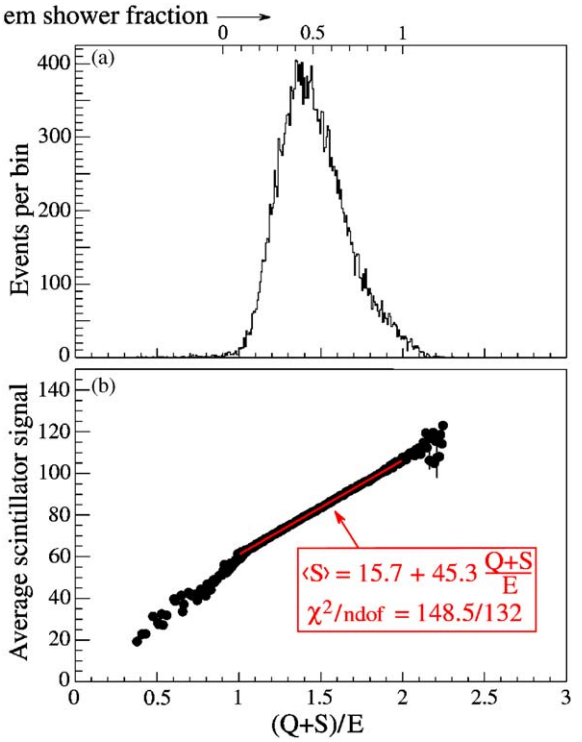

Fig. 14. Distribution of the variable $(Q+S)/E$, and of the em shower fraction derived on the basis of Eq. (2), for 100 GeV π^- showering in the DREAM calorimeter (a). The average scintillator signal for 100 GeV π^-, as a function of $(Q+S)/E$ (b).

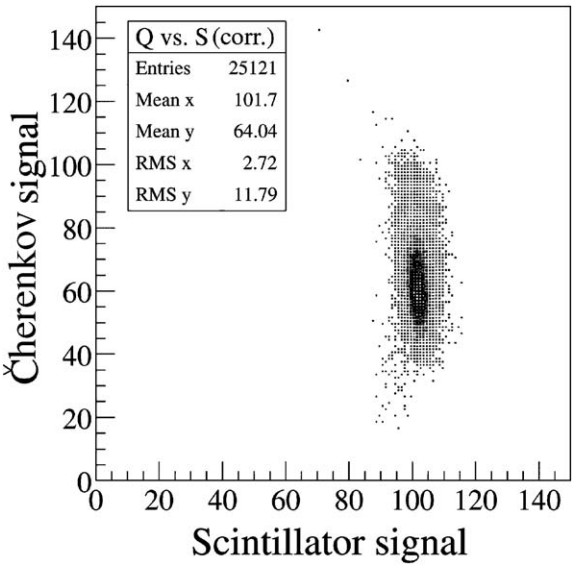

Fig. 15. Cherenkov signals versus scintillator signals for 100 GeV π^- in the DREAM calorimeter, after the correction given in Eq. 4 has been applied.

the measured scintillator signals, as follows:

$$\left(\frac{S}{E}\right)_{\text{corr}} = \left(\frac{S}{E}\right)_{\text{meas}} + 0.453\left[1.9 - \frac{Q+S}{E}\right] \qquad (4)$$

where 0.453 is the fitted slope shown in Fig. 14b. Fig. 15 depicts the effect of this correction procedure. The projection of this scatter plot on the horizontal axis, i.e. the signal distribution for the 100 GeV π^- showers after correction, is shown in Fig. 16b. The corrected signal distribution is very well described by a Gaussian fit, with a σ/mean of 2.6%, a large improvement with respect to the energy resolution of 12.3% measured before correction (Fig. 16a).

Fig. 17 shows the energy dependence of these results, obtained by using Eq. (4) at all energies. Results are shown for data sets 1 and 2 (see Section 4.1). The square of the resolution is plotted vs. E^{-1} in this figure. This is done to make it easy to see how the experimental data are described by an expression of the type

$$\frac{\sigma}{E} = \frac{a}{\sqrt{E}} \oplus b \qquad (5)$$

i.e. , the quadratic sum of a stochastic and a constant term, which is represented by a straight line in this plot. Both sets of data are well described by Eq. (5), with $a \sim 20\%$ in both cases, while differing in the value of b. As in the case of em showers [12], deviations from $E^{-1/2}$ scaling expressed by a constant term are caused by sampling non-uniformities depending on the impact point of the particles, i.e. depending on whether the particles enter the detector in the copper absorber or in a fiber area. As in the case of em showers, these non-uniformities are very sensitive to the orientation of the detector. They increase steeply when the angle between the fibers and the direction of the incoming particles approaches zero. In the "untilted" case, where the angle between the fibers and the incoming particles amounted to 2.1°, the constant term b

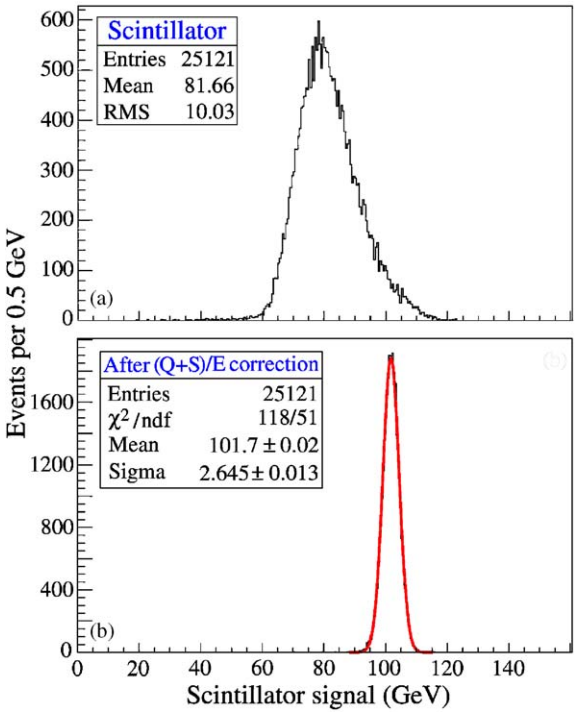

Fig. 16. Scintillator signal distributions for 100 GeV π^- showers in the DREAM calorimeter, before (a) and after (b) the correction described in Eq. (4).

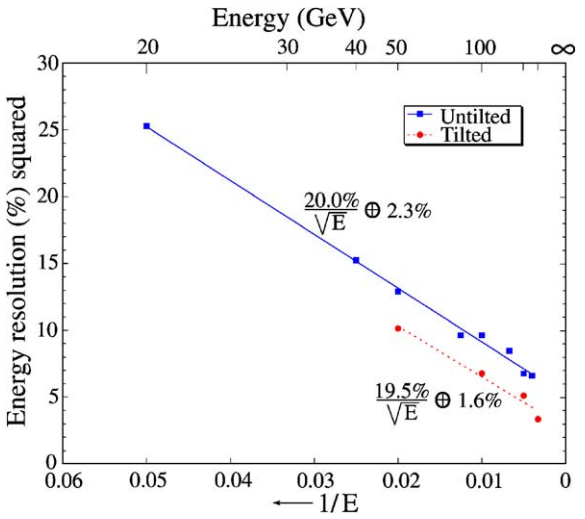

Fig. 17. The squared energy resolution $(\sigma/E)^2$ as a function of the pion energy, after the correction described in Eq. (4) was applied to the scintillator signals. Results are given for the DREAM calorimeter oriented in the "tilted" and "untilted" positions.

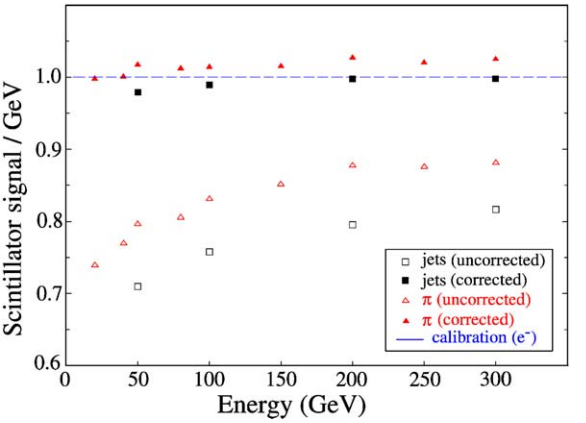

Fig. 18. The scintillator response of the DREAM calorimeter to single pions and "jets", before and after the correction described in Eq. (4) was applied to the signals.

was measured to be 2.3%, in the "tilted" orientation, where that angle was increased to 3.6°, b was reduced to 1.6%.

The correction procedure (4) also restored signal linearity for hadrons. As is illustrated in Fig. 18, the response is constant, and equal to that of electrons to within a few percent, after the procedure has been applied.

5.2. Jets

As discussed in Section 3.1.4, jet events were mimicked by selecting hadron interactions in the polyethylene target installed upstream of the DREAM calorimeter. The signal measured in the ITC installed in between the interaction target and the calorimeter was used as a measure for the jet multiplicity (see Fig. 6). In the following, we refer to "high-multiplicity jets" as those events in which the ITC signal was larger than 28 mip (the overflow in Fig. 6).

The fact that we are looking at multiparticle events is clearly illustrated in Fig. 19, which shows the distribution of the longitudinal center-of-gravity of the scintillation light produced in the DREAM calorimeter for 200 GeV high-multiplicity "jets". For comparison, the figure also shows the distribution for 200 GeV pions. The latter events were derived from the same data set as the jets (data set 3). Events with a signal in the ITC

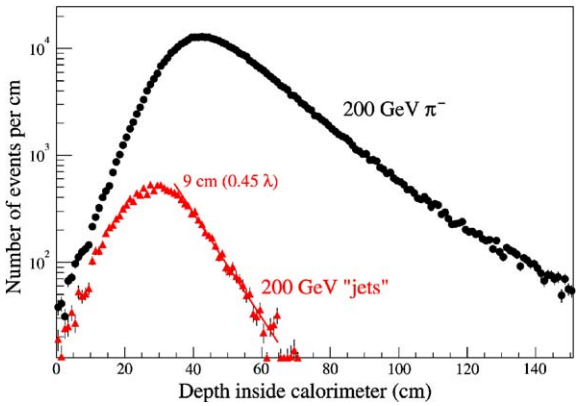

Fig. 19. Distribution of the depth of the center-of-gravity of the scintillation light produced in the DREAM calorimeter by 200 GeV π^- and by high-multiplicity "jets" of the same energy.

between 0.5 and 1.5 mip were selected for this purpose. The depth of the light production (i.e. , the effective z-coordinate of the shower) was measured as described in Section 4.2. The figure shows that the jets, on average, generated light closer to the front face than single pions. Also, the event-to-event spread in the z-value is much smaller for the jets, and the trailing slope of their distribution is steeper.

These effects are due to the fact that the "jets" are a collection of photons and pions, each with an energy considerably smaller than 200 GeV. The photons develop em showers and deposit their energy therefore almost entirely in the first $20X_0$ (40 cm). The pions penetrate deeper, but since there are many of them, the fluctuations in the longitudinal shower development, which are of the order of $1\lambda_{\text{int}}$ for single pions (Fig. 7), are effectively reduced by a factor $\sqrt{n}$, n being the number of hadron showers developing simultaneously. Since, the slope of the jet distribution is well described by an exponential with a coefficient of $0.45\lambda_{\text{int}}$, the effective value of n is ~ 5 in this data sample.

The fact that the jets consist of a number of particles showering simultaneously has also interesting consequences for the response function. Fig. 20a shows the scintillator signal distribution for high-multiplicity 200 GeV "jets". This distribution is considerably more symmetric than that

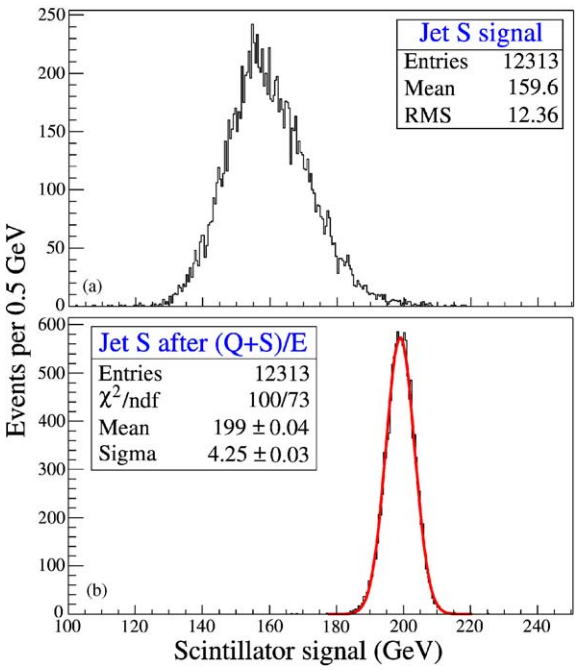

Fig. 20. Scintillator signal distributions for 200 GeV high-multiplicity "jets" in the DREAM calorimeter, before (a) and after (b) the correction described in Eq. (4) was applied to the signals.

for 200 GeV pions (Fig. 16a). The reduced χ^2 of a Gaussian fit to both distributions was found to be 94 for single pions vs. 2.0 for the jets (for ~ 150 degrees of freedom). This phenomenon is a consequence of the Central Limit Theorem.

The resolution for the jets is also considerably better than that for single pions of the same energy. Fluctuations in the energy carried by the em shower fraction, which dominate this resolution, are apparently smaller for the jets. In the case of single pions, a single π^0 created in the first interaction may carry an anomalously large fraction of the total energy. This process has no equivalent for our "jets", where the energy is distributed over a large number of particles.

The extent of the described effects depends on the jet multiplicity. This is illustrated in Fig. 21, which shows that both the energy resolution and the quality of a Gaussian fit to the signal distribution gradually improve with increasing multiplicity.

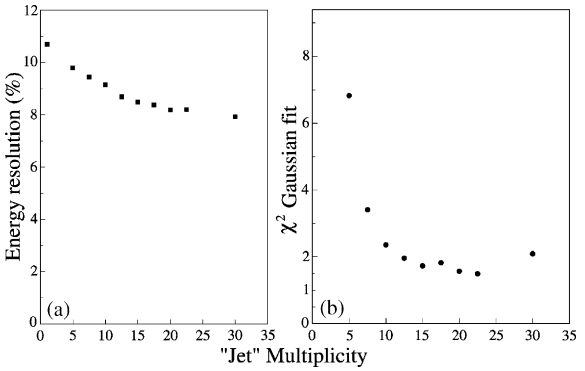

Fig. 21. The energy resolution (a) and the reduced χ^2 (b) of a Gaussian fit to the signal distribution for 200 GeV "jets", as a function of the multiplicity. A multiplicity of 1 refers to single pions, not interacting in the interaction target. The reduced χ^2 for the latter case (off scale) is 94.

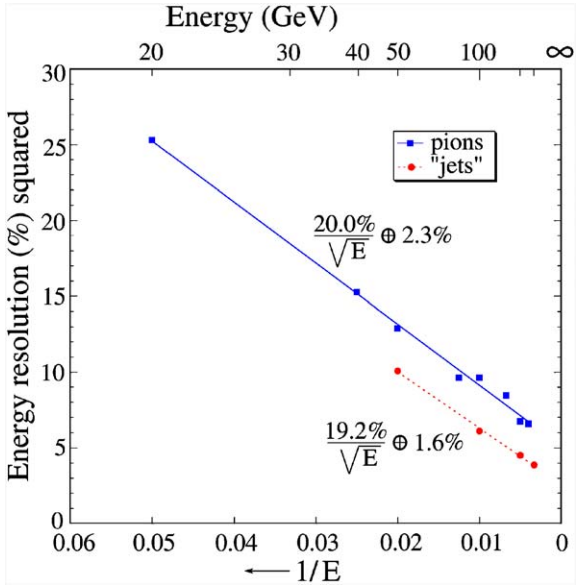

Fig. 22. The squared energy resolution $(\sigma/E)^2$ as a function of energy, after the correction described in Eq. (4) was applied to the scintillator signals. Results are given for single pions and high-multiplicity "jets" detected with the DREAM calorimeter oriented in the "untilted" position, $A(2^\circ, 0.7^\circ)$.

We used the method described for single pions in exactly the same way to improve the energy resolution of jets. Some results are shown in Figs. 18, 20 and 22. After correcting the scintillator signals according to Eq. (4), the signal distribution for 200 GeV jets (Fig. 20a) is transformed into the one shown in Fig. 20b, an almost perfectly Gaussian distribution with a relative width of 2.1% and a mean value of 199 GeV. The energy dependence of the response and of the energy resolution are shown in Figs. 18 and 22, respectively. Fig. 18 illustrates that, as in the case of single pions, Eq. (4) restores signal linearity for jets to within a few percent. Fig. 22 shows that the jet energy resolution after the correction is well described by the quadratic sum of a $E^{-1/2}$ stochastic term and an energy independent term (Eq. (5)). The stochastic term is approximately the same as for single pions ($19-20\%/\sqrt{E}$), whereas the constant term is significantly smaller (1.6% for jets vs. 2.3% for pions). In Section 5.1, we saw that this constant term is mainly the result of sampling non-uniformities. Since the shower energy is spread out over more fibers in the case of jets, these non-uniformities have a smaller effect than for single pions. For example, on average 41% of the energy of 200 GeV "jets" is deposited outside the central tower, vs. 35% for single pions of the same energy.

5.3. The Q/S method

In the previous subsections, we saw that the correction based on Eq. (4) led to an energy-independent response (signal linearity), equal response for em and hadronic showers, Gaussian signal distributions and excellent energy resolutions, both for single pions and for jets. However, Eq. (4) depends on knowledge of the particle (or jet) energy, E. Unlike in beam tests, this energy is in practice unknown in most particle physics experiments. Therefore, we have looked for alternative methods that do *not* rely upon knowledge of the energy of the incoming particles. One such method, discussed in this subsection, is based on the measured *ratio* of the two different signals generated by our calorimeter: Q/S.

The hadronic resolution of this calorimeter is affected by at least five factors:

(1) Photoelectron statistics,
(2) Sampling fluctuations,

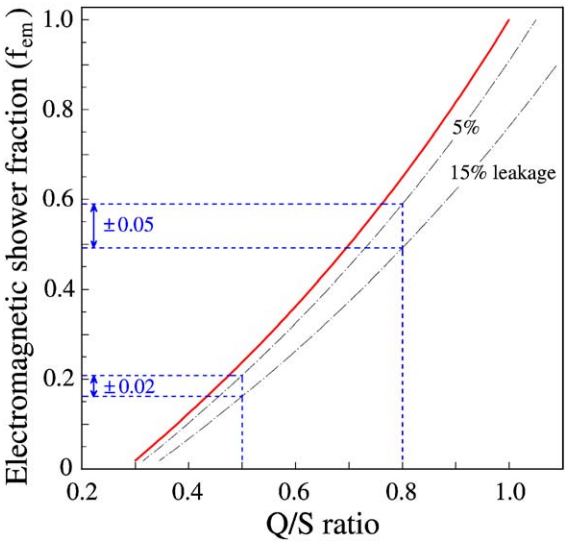

Fig. 23. The relationship between the Q/S signal ratio and the em shower fraction, f_{em}. Also shown is how a shower leakage of $10 \pm 5\%$ translates into an uncertainty in the em shower fraction.

(3) Fluctuations in visible energy resulting from nuclear breakup,
(4) Fluctuations in visible energy resulting from shower leakage, and
(5) Fluctuations in em shower content (f_{em}).

By assuming knowledge of E, factors 3 and 4 are by definition eliminated, while Eq. (4) eliminates the effects of the fifth factor. As a result, the correction method described in the previous subsections reduced the resolution to the effects of sampling fluctuations and photoelectron statistics. Any method intended to be independent of knowledge of E will have to address the effects of leakage fluctuations.

This is illustrated in Fig. 23, which exhibits the relationship between the em shower fraction, which we need to correct the calorimeter signals for the effects of non-compensation, and the Q/S signal ratio, which is measured. The solid curve represents Eq. (2), which describes this relationship for e/h values of 1.4 and 5.0 for the scintillating and Cherenkov calorimeter structures, respectively. The figure also shows how this relationship is affected when shower leakage plays a role. Since, the non-relativistic shower particles which do contribute to the scintillator signals but not to the Cherenkov ones are predominantly found in the tails of the shower profiles [1], the scintillator signals in this narrow calorimeter are much more affected by leakage than the Cherenkov ones. Two additional curves show the modified relationship when 5% or 15% of the scintillator signal goes undetected because of shower leakage (assuming no leakage in the Cherenkov channel). As illustrated in the figure, uncertainty in the shower leakage translates directly into an uncertainty in the value of the em shower fraction (f_{em}), and thus in the precision of corrections based on this value.

We studied several variables that might provide information about shower leakage on an event-by-event basis. The most promising variable turned out to be the fraction of the total scintillator signal that was observed in the Outer Ring, f_{out}. Based on studies of the radial shower profiles [13], we concluded that there was a useful correlation between f_{out} and the fraction of the signal that went undetected because of the limited lateral size of the calorimeter. The measured scintillator signals, S_{meas}, were corrected event by event for the effects of lateral shower leakage, as follows:

$$S_{corr} = S_{meas}(1 + x f_{out}) \tag{6}$$

in which the value of x was chosen to be 1.0, for all energies. There was no difference in the correction procedure for single particles and jets, the x value was the same in both cases. However, since the lateral profiles for jets were broader than for single pions, the average value of f_{out}, and thus the average correction for lateral shower leakage, was larger. The corrections were also, on average, larger at low energy than at high energy. Since the Cherenkov profiles are narrower than the scintillator ones, no leakage corrections were applied to the Cherenkov signals.

After the signals were corrected with Eq. (6) for the effects of shower leakage, the scatter plot for 100 GeV π^- events (Fig. 12) transformed into the one shown in Fig. 24a. As before, a fixed value for the Q/S signal ratio corresponds to a line

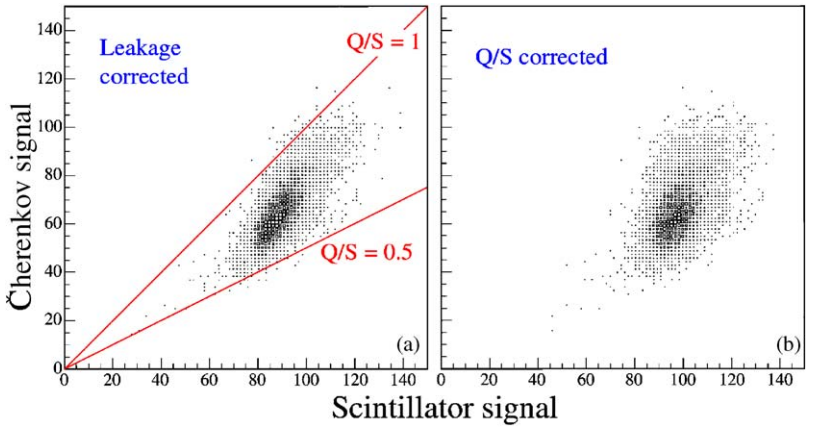

Fig. 24. Cherenkov signals versus scintillator signals for 100 GeV π^- in the DREAM calorimeter. These plots were derived from the raw data (Fig. 12) after applying corrections for shower leakage, using Eq. (6) (a) and, in addition, for the effects of non-compensation, using Eq. (7) (b).

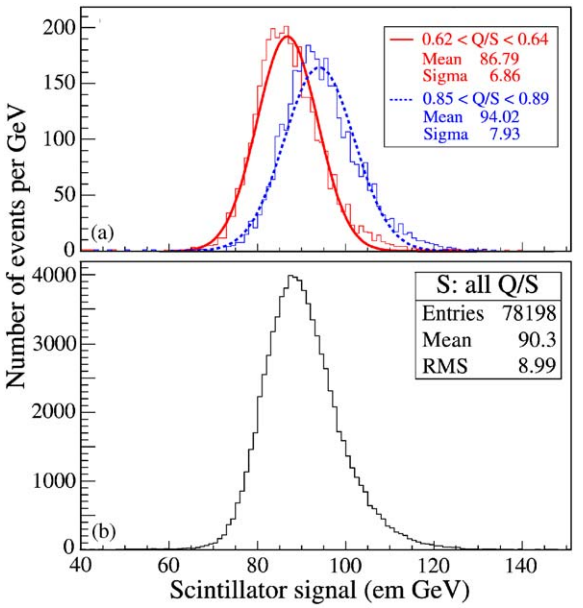

Fig. 25. Scintillator signal distributions for 100 GeV π^- in the DREAM calorimeter. The distributions for events within two narrow Q/S bands (a) are compared with the total distribution obtained after correcting, event by event, for the effects of shower leakage (b).

through the origin of the scatter plot. The two lines drawn in this figure represent $Q/S = 1$ and 0.5, respectively.

Fig. 25 illustrates the fact that there is merit in this Q/S ratio. The scintillator signal distributions for two event samples selected on the basis of the measured Q/S signal ratio are shown in Fig. 25a. The first sample concerns events with $0.62 < Q/S < 0.64$, the second sample events with $0.85 < Q/S < 0.89$. Both distributions are narrower than the total (leakage corrected) distribution, i.e. the projection of the scatter plot from Fig. 24a on the horizontal axis, which is shown for comparison in Fig. 25b. The mean value of the distribution clearly increases with the value of Q/S, which is to be expected since the response increases with the em fraction. And finally, the asymmetry of the response function is greatly reduced in these distributions.

The procedure to exploit these features for improving the hadronic calorimeter performance was the same for single pions and for jets. In the following, we illustrate the entire procedure for the 200 GeV high-multiplicity "jets", created by pions interacting in the upstream target. Starting from the measured signals in the scintillator and Cherenkov channels, this procedure consists of the following steps.

(1) First, the scintillator signals are corrected for the effects of lateral shower leakage, using Eq. (6). Fig. 26 shows the distribution of the

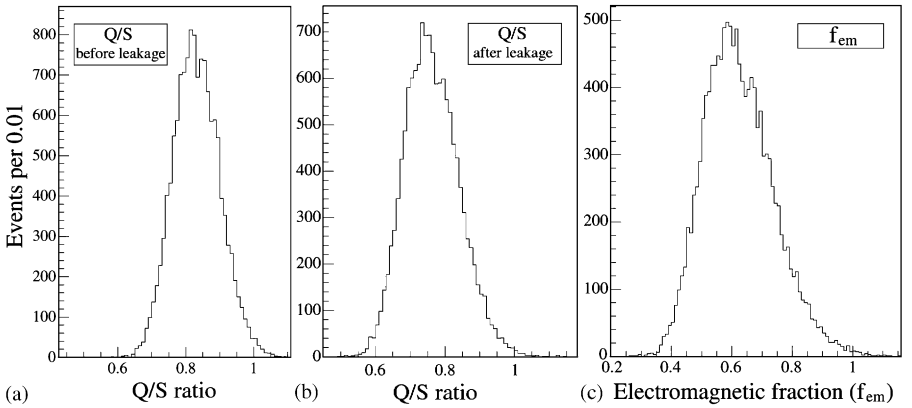

Fig. 26. Distribution of the em shower fraction (f_{em}) for 200 GeV high-multiplicity "jets" (c), derived from the Q/S signal ratio (a), after corrections for shower leakage have been applied (b).

Q/S signal ratio before (Fig. 26a) and after (Fig. 26b) this correction was made. On average, the scintillator signals increased by $\sim 10\%$ as a result of this correction, so that the average Q/S value decreased from 0.83 to 0.76.

(2) Next, the (leakage corrected) Q/S signal ratio is converted into an f_{em} value. We used Eq. (2) for this purpose, using $e/h = 1.3$ (for reasons explained below) and 5.0 for the scintillating and Cherenkov calorimeter structures, respectively. Fig. 26c shows the resulting f_{em} distribution for these "jets". This distribution exhibits the characteristic asymmetric shape that is reflected in the calorimeter response function, but for reasons discussed in Section 5.2 it is much less pronounced than for single pions (cf. Fig. 14a). The average em shower fraction was about 62% for these jets.

(3) Once the value of f_{em} is known, corrections for the effects of non-compensation are applied to the scintillator signals with the following formula:

$$S_{\text{final}} = S_{\text{corr}}\left[\frac{1+p_1/p_0}{1+f_{em}p_1/p_0}\right], \quad \text{with } \frac{p_1}{p_0} = \frac{e}{h} - 1 \tag{7}$$

in which S_{corr} represents the leakage-corrected scintillator signal.

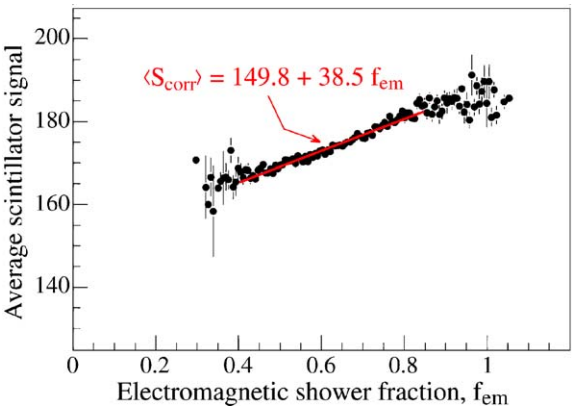

Fig. 27. The average (leakage-corrected) scintillator signal for 200 GeV jets, as a function of the em shower fraction, f_{em}.

The validity of Eq. (7) and the experimental meaning of the ratio p_1/p_0 can be seen as follows. If we rewrite Eq. (1) as

$$R(f_{em}) = p_0 + p_1 f_{em} \tag{8}$$

the relationship between the e/h ratio and p_1/p_0 given in Eq. (7) follows immediately. The ratio p_1/p_0 describes the f_{em} dependence of the hadronic response R of a non-compensating calorimeter, and thus the f_{em} dependence of the average calorimeter signal. Fig. 27 shows the relationship between the average scintillator signal $\langle S_{corr} \rangle$ and f_{em} for 200 GeV "jets". There is indeed a linear

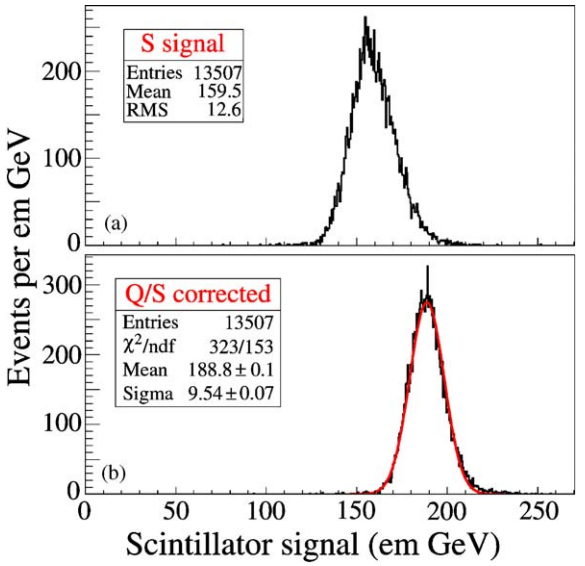

Fig. 28. Scintillator signal distributions for 200 GeV high-multiplicity "jets" in the DREAM calorimeter before (a) and after (b) the corrections based on the observed Q/S signal ratio were applied.

relationship, although the slope is somewhat smaller than expected. The ratio $p_1/p_0 = 38.5/149.8 = 0.26$ instead of 0.40 (i.e. $1.4-1$). This indicates that the e/h value of our scintillator calorimeter is $\sim 1.25-1.3$ rather than 1.4 as assumed above. Measurements at other energies confirmed this, a linear fit to the data consistently yielded p_1/p_0 values in the 0.25–0.30 range. For this reason, we used $e/h = 1.3$ to convert Q/S ratios into f_{em} values.

In order to correct for the effects of non-compensation, the (leakage-corrected) calorimeter signal has to be increased such as to make the response equal to that for em showers: $R = 1$. This means that

$$\frac{S_{\mathrm{final}}}{S_{\mathrm{corr}}} = \frac{1}{R(f_{\mathrm{em}})} = \frac{1}{f_{\mathrm{em}} + (e/h)^{-1}(1-f_{\mathrm{em}})} = \frac{e/h}{f_{\mathrm{em}}e/h + 1 - f_{\mathrm{em}}} \tag{9}$$

and this leads to the correction formula given in Eq. (7). Fig. 28 shows the effect of these corrections for the 200 GeV high-multiplicity "jets".

In the analysis described above, we have used the measured f_{em} values to improve the calorimeter performance in the scintillator channel. However, the information can equally well be used to correct the Cherenkov signals for the effects of non-compensation. In fact, a comparison of the results for both channels may serve as an internal consistency check of the method. Since the Cherenkov calorimeter has a much larger e/h value, the effects of non-compensation, and thus the improvements resulting from the Q/S method, are much larger than for the scintillator channel. This is illustrated in Fig. 29, which as before concerns the 200 GeV high-multiplicity "jets". Fig. 29a shows that the average Cherenkov signal depends much more strongly on f_{em} than the average scintillator signal. But also here, the f_{em} dependence is well described by a straight line. The value of p_1/p_0 was found to be $148/40 = 3.7$, which means that $e/h = 4.7$, in good agreement with the value of 5 we assumed for this analysis. Figs. 29(b) and (c) show how application of the correction formula (Eq. (7)), using this value of p_1/p_0 and the measured f_{em} values, transforms the Cherenkov signal distribution. The final result (Fig. 29c) looks remarkably similar to the corrected scintillator signal distribution (Fig. 28b), in terms of average value (190.1 vs. 188.8 GeV), resolution ($\sigma/E = 5.09\%$ vs. 5.05%) and line shape ($\chi^2 = 292/158$ vs. 323/153).

In both cases, the corrections have the following effects:

- The average value of the corrected signal distribution is close to 200 GeV, the energy of the beam particles that generated the "jets" (Fig. 31).
- The corrected signal distribution is much more symmetric than the uncorrected one.
- The energy resolution is considerably improved. Deviations from $E^{-1/2}$ scaling, characteristic of non-compensating calorimeters, have been largely eliminated.

The latter effect is illustrated in Fig. 30, which shows the resulting energy resolution for

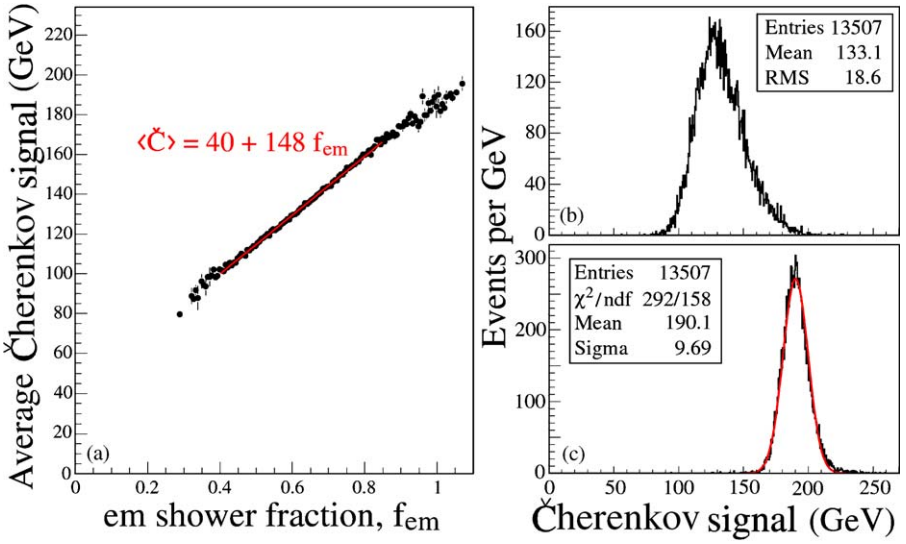

Fig. 29. The average Cherenkov signal for 200 GeV jets, as a function of the em shower fraction, f_{em} (a). Cherenkov signal distributions for 200 GeV high-multiplicity "jets" in the DREAM calorimeter before (b) and after (c) the corrections based on the observed Q/S signal ratio were applied.

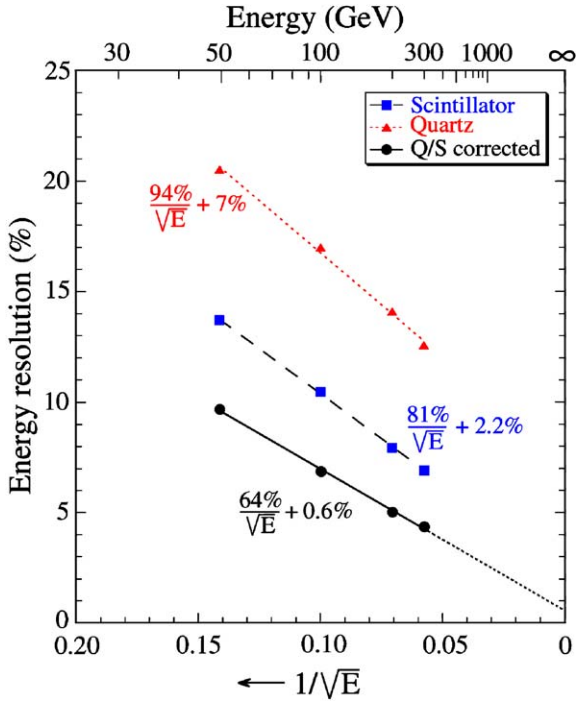

Fig. 30. The jet energy resolution as a function of energy, measured with the scintillation fibers and the Cherenkov fibers, and after corrections made on the basis of the measured Q/S signal ratio.

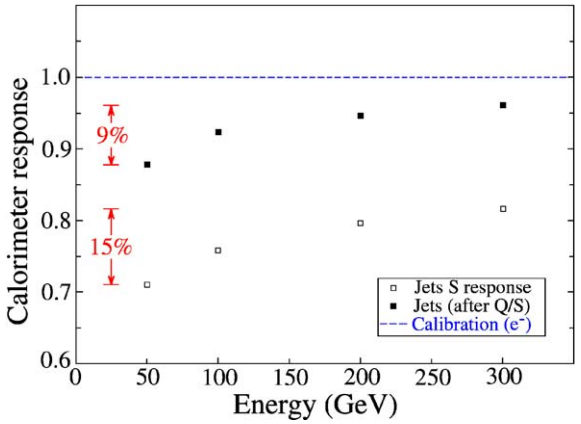

Fig. 31. The scintillator response to high-multiplicity jets, before and after corrections made on the basis of the measured Q/S signal ratio.

high-multiplicity "jets". As explained in Ref. [1], the effects of non-compensation on the hadronic energy resolution manifest themselves as a constant term, to be added *linearly* to the stochastic term. The lines drawn through the points in Fig. 30, which represent fits of this type, describe the data reasonably well. A fit to the Q/S

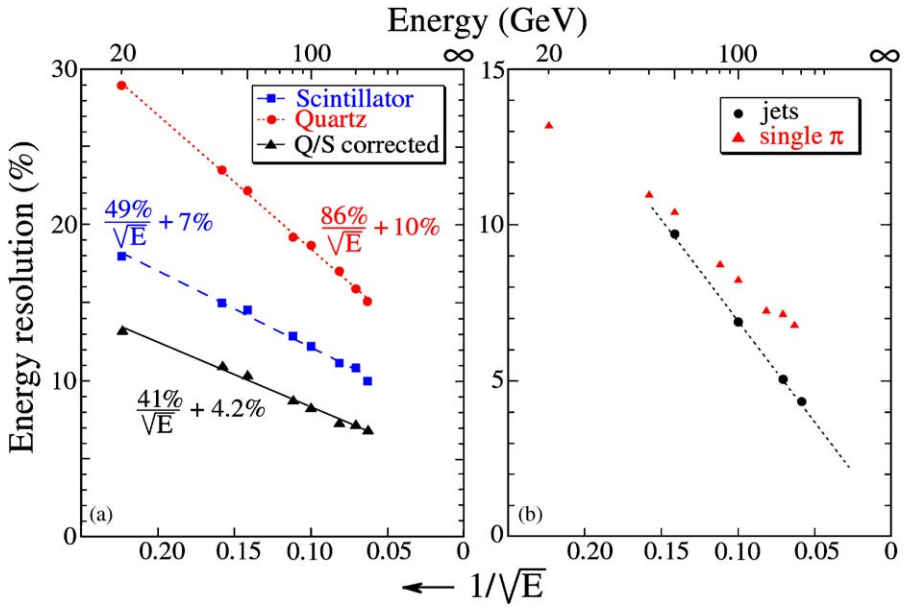

Fig. 32. The energy resolution for single pions as a function of energy, measured with the scintillation fibers and the Cherenkov fibers, and after corrections made on the basis of the measured Q/S signal ratio (a). Comparison of the corrected resolutions for jets and single pions (b).

corrected jet data gave the following result:

$$\sigma/E = \frac{64\%}{\sqrt{E}} + 0.6\%$$

This illustrates that the effects of non-compensation on the jet energy resolution have been almost completely eliminated. At the highest energies accessible in these tests, we achieved jet resolutions better than 4%. For comparison, the resolutions measured with the two types of fibers before the Q/S correction method was applied are also shown in this figure.

We want to stress that knowledge of the beam energy was *not* used in any stage of the analysis described in this subsection. Yet, the Q/S method also brought the "jet" response much closer to that of electrons, which were used to calibrate the detector. Moreover, it improved the hadronic signal linearity. This can be seen from Fig. 31, which shows the (scintillator) response to "jets" before and after the corrections were applied.

Somewhat surprisingly, the resolution for single pions did not benefit as much from the Q/S correction method as the resolution for "jets".

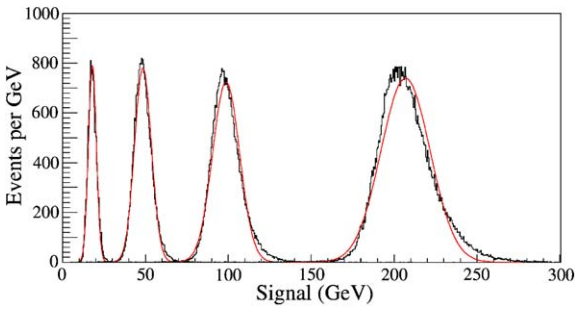

Fig. 33. Q/S-corrected scintillator signal distributions for single pions at 20, 50, 100 and 200 GeV. The curves represent Gaussian fits.

This is illustrated in Fig. 32. Most likely, this is due to the effects of *longitudinal* shower leakage. A detector of this type is extremely sensitive to such leakage, since the fibers exiting from its rear represent a region with a sampling fraction of 100%, compared to 2% for the detector itself. Therefore, any longitudinal leakage is strongly amplified in the signals [14]. This explanation is supported by the fact that the asymmetry in the

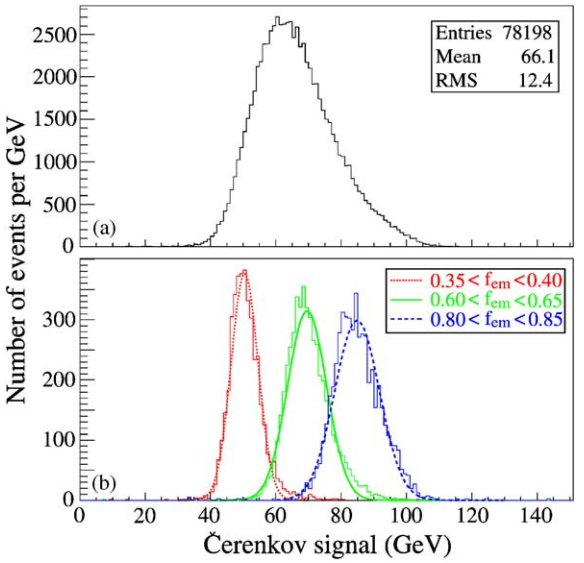

Fig. 34. Cherenkov signal distribution for 100 GeV π^- (a) and distributions for subsamples of events selected on the basis of the measured f_{em} value, using the Q/S method (b).

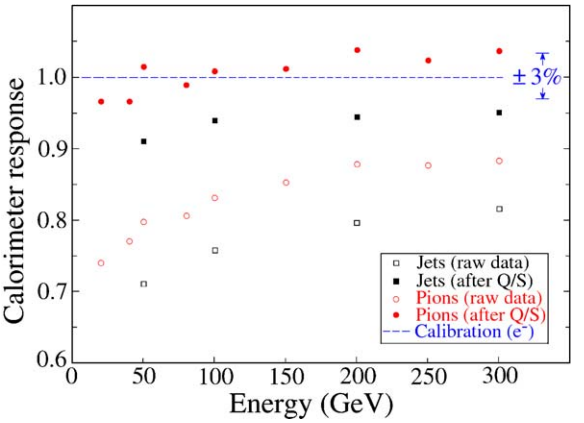

Fig. 35. The calorimeter response to single pions and high-multiplicity jets, before and after corrections made on the basis of the measured Q/S signal ratio.

signal distributions, although greatly reduced, was not completely eliminated, especially at the highest energies. This is illustrated in Fig. 33.

Also the fact that the detector was oriented at a small angle with respect to the beam particles may have contributed to these phenomena. Particles penetrating deep inside the detector before starting a shower deposit a larger than average fraction of their energy in the Outer Ring, which leads to leakage corrections that are too large.

The above explanations are further corroborated by the fact that the asymmetry disappeared when events were selected in which the center-of-gravity of the light production was located closer to the front face of the detector (see Section 4.2). Since the "jets" used for this analysis deposited their energy, on average, much more upstream in the detector than the single pions (see Fig. 19), they were not affected by the described effects. Fig. 32b shows that the difference between the resolutions for jets and single pions indeed increases with energy.

Nevertheless, also the energy resolution for single pions benefited considerably from the corrections made on the basis of the measured Q/S signal ratio. Fig. 34 shows how subsamples of events selected on the basis of the f_{em} value derived from this ratio clearly probed different regions of the Cherenkov signal distribution for 100 GeV π^-. Even though not perfect, these distributions are considerably more symmetric than the overall distribution.

We have found that a more sophisticated treatment of the corrections for shower leakage further improves the results. For example, when we replaced Eq. (6) by

$$S_{corr} = S_{meas}\left[1 + 0.2\left[1 - \exp(-yf_{out}/\sqrt{S_{meas}})\right]\right] \quad (10)$$

with $y = 60$, linearity was restored to within ±3%, both for single pions and for jets (Fig. 35), while also the quality of the Gaussian fits improved.

We did not engage in a systematic study to optimize the detector performance through the specific choice of the leakage corrections. However, since a correct description of the effects of shower leakage is apparently important for the results, further improvements of the performance of this type of calorimeter may be expected if the dimensions of the detector are increased, both laterally and (for single particles) longitudinally.

Quantitative information in this respect may be derived from SPACAL studies [2], in which the

contribution of lateral shower leakage to the hadronic energy resolution was measured to be well described by the following expression:

$$\sigma/E = x\sqrt[4]{E} \quad (11)$$

where x is the (energy-dependent) average fraction of the energy that leaks out. When applied to the DREAM detector, this formula indicates that leakage fluctuations contributed more than half of the measured energy resolution, for the entire jet energy range studied here. Fluctuations in visible energy resulting from nuclear binding energy losses account for the remainder of the difference between the measured resolution and the "ideal" one (Fig. 22). In realistic conditions, where the beam-energy constraint (Eq. (4)) cannot be used, the latter, irreducible, fluctuations will inevitably contribute to and limit the achievable jet resolutions.

6. Conclusions

We have tested a novel type of hadronic sampling calorimeter, equipped with two independent active media. This design was based on the idea to simultaneously measure dE/dx (in the form of scintillation light) and the production of Cherenkov light in the shower development. The latter is almost exclusively generated by the electromagnetic shower components and, therefore, a comparison of the two signals makes it possible to determine the fraction of the shower energy deposited in em form (f_{em}) *event by event*. Since fluctuations in f_{em} are responsible for the poor performance of non-compensating calorimeter systems, and since these (dominant) fluctuations can be eliminated with this method, the performance of our detector is superior to what is commonly achieved with calorimeters used in particle physics experiments.

For example, the energy resolution for jets was found to scale almost perfectly with $E^{-1/2}$. Deviations from such scaling in the energy range from 50 to 300 GeV were less than 1% ($\sigma/E = 64\%/\sqrt{E} + 0.6\%$). The corrections applied to the signals, based on the Q/S signal ratio, also led to an approximately correct reconstruction of the hadronic shower energy (in an instrument calibrated with electron showers) and greatly reduced the hadronic signal non-linearity that is typical for non-compensating calorimeters. This was true both for single pions and for jets, which were treated in exactly the same way in our analyses.

The tested detector was very small, its total instrumented mass was only 1030 kg. As a result, fluctuations in shower leakage accounted for more than half of the measured jet resolutions, at all energies. We have shown that if we made use of the fact that the energy of the showering particle was known (thus effectively eliminating the contributions of shower leakage and of nuclear binding energy losses), the mentioned resolution could be greatly improved.

In the analyses described in this paper, we have not made an effort to optimize the performance of the tested instrument. We have evidence that, for example, a more sophisticated treatment of the shower leakage corrections would yield even better results than the ones presented here. Rather, we wanted to focus on the fundamentals of the dual-readout method and on *how* the information it provides can be employed to improve the performance of hadron calorimeters.

Acknowledgements

We gratefully acknowledge the contributions of Tracy McAskill, Vladimir Nagaslaev, Alan Sill, Veronica Stelmakh, Yunyong Wang, Erika Washington and Kim Zinsmeyer to the construction of the DREAM detector. We thank CERN for making particle beams of excellent quality available. Our beam tests would not have been possible without the help we received from Claude Ferrari and Maurice Haguenauer. We thank K. Kuroda for loaning us the fiber hodoscopes, and A. Gorin and I. Manouilov for their assistance with the data acquisition system. This study was carried out with financial support of the United States Department of Energy, under contract DE-FG02-95ER40938, and the Advanced Research Program of the State of Texas.

References

[1] R. Wigmans, Calorimetry—Energy Measurement in Particle Physics, International Series of Monographs on Physics, vol. 107, Oxford University Press, Oxford, 2000.
[2] D. Acosta, et al., Nucl. Instr. and Meth. A 308 (1991) 481.
[3] W. Braunschweig, et al., Nucl. Instr. and Meth. A 265 (1988) 419;
W. Braunschweig, et al., Nucl. Instr. and Meth. A 275 (1989) 246.
[4] M. Albrow, et al., Nucl. Instr. and Meth. A 487 (2002) 381.
[5] V.L. Morgunov, Proceedings of the 10th International Conference on Calorimetry in High Energy Physics, Pasadena, March 25–29, 2002, p. 70.
[6] D. Buskulic, et al., Nucl. Instr. and Meth. A 360 (1995) 481.
[7] O. Lobban, A. Sriharan, R. Wigmans, Nucl. Instr. and Meth. A 495 (2002) 107.
[8] H. Abramowicz, et al., Nucl. Instr. and Meth. A 180 (1981) 429.
[9] N. Akchurin, et al., Nucl. Instr. and Meth. A 399 (1997) 202.
[10] V.P. Nagaslaev, A.F. Sill, R. Wigmans, Nucl. Instr. and Meth. A 462 (2000) 411.
[11] F.G. Hartjes, R. Wigmans, Nucl. Instr. and Meth. A 277 (1989) 379.
[12] N. Akchurin, et al., Electron detection with a dual-readout calorimeter, Nucl. Instr. and Meth., accepted for publication.
[13] N. Akchurin, et al., Comparison of high-energy shower profiles measured with scintillation and Cherenkov light, Nucl. Instr. and Meth., accepted for publication.
[14] D. Acosta, et al., Nucl. Instr. and Meth. A 294 (1990) 193.